Formation and decay of the spring warm pool in the South China Sea

Weiqiang Wang[1] and Chunzai Wang[2]

[1]   As part of the southeast Asian monsoon system, the South China Sea (SCS) is characterized by monsoon wind transition from northeasterly to southwesterly in the boreal spring. Correspondingly, a spring warm pool (SWP) with mixed layer temperature warmer than 29°C is formed and peaked in May over the central SCS and then decays in June. Calculations of the heat budget showed that the surface heat flux and ocean dynamics have different roles in the formation and decay of the SWP. The surface heat flux is found to play a dominant role for the formation of the SWP in May. The onset of the southwest monsoon corresponds to an increase in cloudiness and rainfall and a strong wind speed in the SCS that decrease the surface heat flux in June. Moreover, the onset of the southwest monsoon also changes oceanic circulation pattern that advects cold water from the northwest to the southeast and pumps cold water into the upper mixed layer. These cooling effects overcome the warming effect of the surface heat flux, resulting in the decay of the SWP in June. **Citation:** Wang, W., and C. Wang (2006), Formation and decay of the spring warm pool in the South China Sea, *Geophys. Res. Lett.*, *33*, L02615, doi:10.1029/2005GL025097.

1. Introduction

[2]   The South China Sea (SCS) is a large tropical marginal sea, connected to the western Pacific Ocean and the eastern Indian Ocean via a series of narrow and shallow sea straits. As part of the Indo-Pacific warm pool that plays a significant role in the formation and development of the Southeast Asian monsoon [e.g., *Lau and Lau*, 1992; *Chu et al.*, 1997; *Lau et al.*, 2000], warm water over the SCS has a large variation. The seasonal variation of warm water in the SCS has been previously studied by using both observations and numerical models [e.g., *He and Guan*, 1997; *Zhao and Chen*, 2000; *Zhang et al.*, 2001; *Liu et al.*, 2002]. In particular, *Xie et al.* [2003] and *Liu et al.* [2004] recently give a comprehensive study of the SCS sea surface temperature (SST) in the boreal summer and winter, respectively using high-resolution satellite measurements.

[3]   During the boreal spring of the seasonal monsoon transition period, the SCS SST increases rapidly. The SCS shows a large area of warm water with mixed layer temperature greater than 29°C which is called the spring warm pool (SWP). The SWP is located in the central SCS and peaks in May, and then decays in June (Figure 1a). *Chu*

et al. [1997] hypothesized that the surface wind stress curl associated with the bottom topography of the SCS might be responsible for the evolution of the SWP. When the surface wind stress curl over the central SCS is anticyclonic, Ekman downwelling leads to the generation of the SWP. This SWP with high oceanic temperature may lower the atmospheric surface pressure, and the low surface pressure induces an atmospheric cyclonic circulation that in turn cools the SWP. The present paper will show that although Ekman downwelling can warm the central SCS in May, it is not a major factor for controlling the formation of the SWP.

[4]   Using historical data, *Qu* [2001] confirmed the existence of the SWP in the SCS. He studied the SWP in a qualitative manner by describing the relationships among SST, surface heat flux, wind stress, mixed layer depth, and entrainment rate during the boreal spring. However, he did not quantitatively examine the heat budget of the SWP. Therefore, the relative importance of processes controlling the SWP evolution remains to be determined. The purpose of the present paper is to investigate physical processes that are responsible for the formation and decay of the SWP in the SCS.

2. Oceanic and Atmospheric Conditions Associated With the SWP

[5]   Before we calculate the heat budget of the SWP, we examine oceanic and atmospheric conditions during April to June in the SCS that will help us understand SWP's mechanisms discussed in next section. Several data sets are used. The first data set is the Levitus climatological data of the ocean temperature, salinity, and mixed layer depth [*Levitus and Boyer*, 1994]. The Levitus climatology is comprised of quality controlled ocean profile data averaged onto a global 1° latitude × 1° longitude grid at fixed standard depths. Based on the Levitus data, we derive the geostrophic flow field using temperature and salinity with a reference level of 1000 m [*Meyers et al.*, 1995]. The second data set is the climatological surface wind data from Southampton Oceanography Centre at http://www.coaps.fsu.edu/RVSMDC/SAC/SOC/index.shtml, which is also on 1° latitude × 1° longitude grid. Another data set is the surface heat flux of *Oberhuber* [1988] in a 2° × 2° horizontal grid.

[6]   Figure 1 shows the mixed layer temperature, surface wind and wind stress curl, net surface heat flux, and mixed layer depth during April to June. The mixed layer temperature is below 29°C in April and is rapidly developed in May with a large area of water warmer than 29°C. Consistent with the SST (not shown), the mixed layer temperature is maximized in May and then decays in June. The variation of the SWP temperature coincides with atmospheric wind. Figure 1b shows that the boreal spring is a transition time for SCS's wind to switch from the winter northeast monsoon to the summer southwest monsoon. Northeasterly

[1]Key Laboratory of Tropical Marine Environmental Dynamics, South China Sea Institute of Oceanology, Chinese Academy of Sciences, Guangzhou, China.
[2]Physical Oceanography Division, Atlantic Oceanographic and Meteorological Laboratory, NOAA, Miami, Florida, USA.
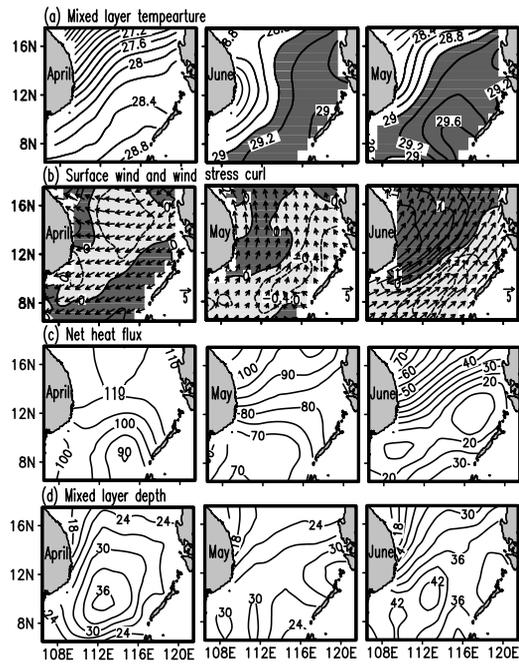
Figure 1. Climatological (a) temperature (°C) averaged over the mixed layer, (b) surface wind (m/s, vectors) and wind stress curl (10^{-7}N/m^3, contours), (c) net surface heat flux (W/m^2), and (d) mixed layer depth (m). The first, second, and third columns show April, May, and June, respectively. In Figure 1a, temperature larger than 29°C is shaded. In Figure 1b, positive (negative) values are in dark (light) shading and with solid (dashed) contour lines.

wind blows over the SCS in April, and the wind starts to change direction in May and by June strong southwesterly prevails in the SCS. Associated with the wind is a negative wind stress curl (Ekman downwelling) in April. Strong southwesterly wind in June divides the SCS into two parts, with a positive and negative wind stress curl in the northwest and southeast, respectively. The contours of the wind stress curl parallels with those of the mixed layer temperature in Figure 1a, indicating that the importance of Ekman pumping in the distribution of the mixed layer temperature.

[7] The net surface heat flux reaches its peak in April in the central SCS and then decays, with the smallest value in June (Figure 1c). The major contributions to the net heat flux in the SCS are shortwave radiation, latent heat flux, and longwave radiation, with sensible heat flux being negligible (not shown). The variation of the surface heat flux in the SCS is also related to the monsoon system. Before the onset of the summer southwest monsoon, the sky over the SCS is relatively clear with less cloud cover and rainfall and thus more shortwave radiation can enter into the upper layer ocean (not shown). At the same time, the loss of the latent heat flux from the ocean is decreased owing to the weak wind during the monsoon transition period of May. Therefore, the net surface heat flux is large over the SCS in April and May (Figure 1c). On the other hand, the onset of the southwest monsoon corresponds to an increase in cloudiness and rainfall in the SCS and thus decreases shortwave radiation. The intensified wind in June (Figure 1b) causes a significant latent heat loss to the atmosphere in the central SCS. The combined effect of the shortwave radiation and

latent heat flux is a small net heat flux which is roughly collocated with the axis of the southwest monsoon wind jet as shown in Figures 1b and 1c.

[8] Atmospheric wind also influences the mixed layer depth through turbulent mixing that requires wind to supply kinetic energy. Since May is a transition month for the monsoon wind to switch from northeasterly to southwesterly, it has a relatively weak wind (Figure 1b). The weak wind cannot provide enough wind kinetic energy to maintain turbulent mixing. As a result, the mixed layer depth reaches its minimum value (<30 m) in May (Figure 1d). The minimum mixed layer depth in May is consistent with that the SWP peaks in May because the shallower the mixed layer is, the more rapidly and easy the mixed layer water is heated.

[9] The mixed layer current includes the Ekman current ($\vec{u}_e = \tau \times k/(\rho f h_m)$) and geostrophic current ($\vec{u}_g$): $\vec{u} = \vec{u}_e + \vec{u}_g$. Figure 2 shows the Ekman current, geostrophic current, and their sum during April to June. Since the wind stress in April and May is relatively weak, the total current for these two months basically follows the geostrophic current. Prominent features of the SCS oceanic circulation are a basin-wide anticyclonic circulation pattern in April and strong southeastward flows south of 12°N in June (Figure 2c). As shown in next section, the southeastward flows play an important role in cooling the SWP.

3. Heat Budget of the SWP

[10] The effect of various physical processes that control the variation of the SWP can be assessed by examining the heat budget over the mixed layer [Qu, 2001]:

$$\frac{\partial T_m}{\partial t} = \frac{Q_{net}}{\rho C_P h_m} - \vec{u} \bullet \nabla T_m - \frac{w_e(T_m - T_d)}{h_m} \qquad (1)$$

where T_m denotes the mixed layer temperature, h_m is the mixed layer depth, Q_{net} is the net surface heat flux, $\vec{u} = \vec{u}_e +$
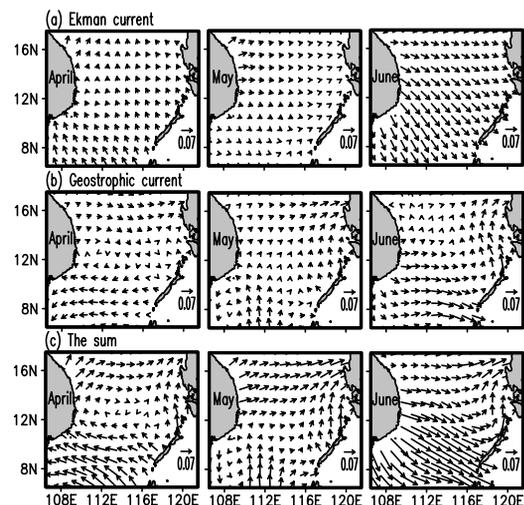
Figure 2. (a) Ekman current, (b) geostrophic current, and (c) sum of the Ekman current and geostrophic current. The first, second, and third columns show April, May, and June, respectively. Unit is m/s.
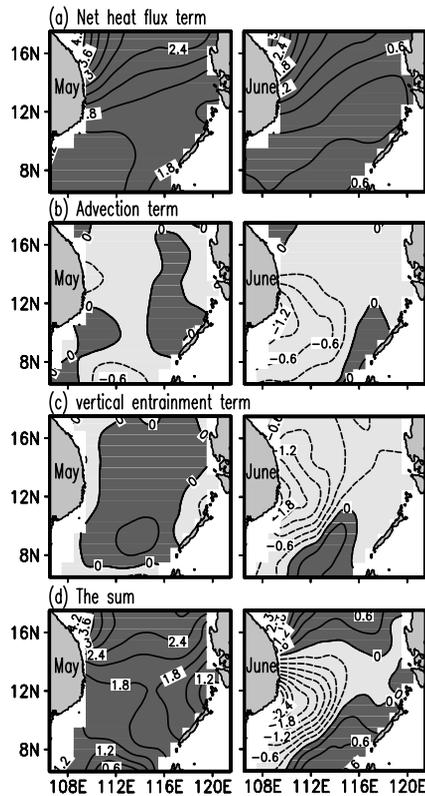
Figure 3. The heat budget of the spring warm pool (SWP). (a) The net heat flux term, (b) horizontal advection term, (c) vertical entrainment term and (d) sum of Figures 3a, 3b, and 3c. The first and second columns show May and June, respectively. Contour interval is 0.3°C/month. Positive (negative) values are in dark (light) shading and with solid (dashed) contour lines.

$\vec{u}_g$, w_e is the entrainment velocity, T_d is the water temperature at a depth of 5m below the base of the mixed layer, and C_p is the specific heat capacity per unit volume. The entrainment velocity w_e, defined as the volume flux of the thermocline water entering the mixed layer per unit horizontal area at the base of the mixed layer, is determined according to the rate of the mixed layer deepening, $\partial h_m/\partial_t$, the vertical velocity of water parcel at the base of the mixed layer, w_{mb}, and the horizontal advection of water parcels below the mixed layer as [e.g., *Cushman-Roisin*, 1987; *Williams*, 1989]:

$$w_e = \frac{\partial h_m}{\partial t} + w_{mb} + \vec{u} \bullet \nabla h_m. \qquad (2)$$

In the SCS where the mixed layer depth is shallow, the vertical velocity at the base of the mixed layer is dominated by Ekman pumping (see *Qu* [2001] for details).

[11] The terms in the right hand side of equation (1) are called the net heat flux, horizontal advection, and vertical entrainment, respectively. Their contributions (individuals and their sum) to the SWP's formation in May and decay in June are shown in Figure 3. In the formation stage of the SWP, the net heat flux is a dominant term for warming the SCS up. The horizontal advection and vertical entrainment are very small. The sum of three terms shows positive

temperature tendency about 1.8°C/month in the central SCS (Figure 3d), which accounts for the formation of the SWP in May.

[12] As stated in the last section, the surface heat flux decreases significantly during June in response to the onset of the summer southwest monsoon. During that time, the contribution of the net surface heat flux decreases to about 0.3°C/month near Palawan Island (Figure 3a). The cooling effect in June results from the horizontal advection and vertical entrainment, all of which are centered in the region east off Vietnam coast (Figures 3b and 3c). Figure 2 shows that after the onset of the summer southwest monsoon, the oceanic flow in the central SCS is southeastward. This southeastward flow, along with the southeastward temperature gradient (Figure 1a), results in the cooling effect of the horizontal advection as shown in Figure 3b. The negative value of the vertical entrainment in Figure 3c is due to the upward entrainment velocity associated with Ekman pumping in June (Figure 1b). The cooling effects of the horizontal advection and vertical entrainment overcome the warming effect of the surface heat flux, resulting in the decay of the SWP in June.

[13] The relative importance of physical processes in controlling the variation of the SWP can be further quantitatively assessed by averaging over the SWP region (defined by the mixed layer temperature larger than 29°C in May). Figure 4 shows the net surface heat flux, horizontal advection, and vertical entrainment averaged over the SWP region. In May, the dominant process for warming the SWP is the surface heat flux. Although the vertical entrainment plays a warming role, its amplitude is very small. The warming tendency (sum of the surface heat flux, horizontal advection, and vertical entrainment) is over 1.5°C/month, consistent with that the SWP peaks in May. However, the situation is different in June. All terms of the net surface heat flux, horizontal advection, and vertical entrainment are comparable in June. The surface heat flux still plays a warming role, whereas the ocean dynamics of the horizontal advection and vertical entrainment cools the SWP. The
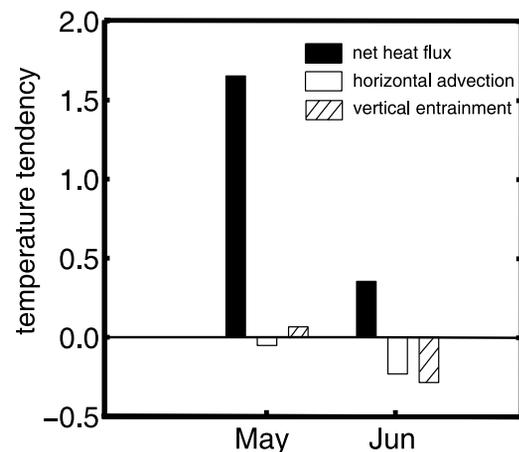
Figure 4. The heat budget averaging over the spring warm pool region (the mixed layer temperature larger than 29°C) during May and June, showing the net heat flux term (black bar), horizontal heat advection term (white bar) and vertical entrainment term (hatched bar). Unit is °C/month.

combined effect is that the cooling effect overcomes the warming effect, resulting in a decay of the SWP in June.

4. Summary

[14] The South China Sea (SCS) is embedded between the western Pacific Ocean and the eastern Indian Ocean. Because of its geographical location, the SCS climate shows the feature of the Southeast Asian monsoon system. In the boreal winter the SCS is dominated by the northeasterly monsoon, whereas in the boreal summer the southwesterly surface wind prevails over the SCS. As the monsoon transition from northeasterly to southwesterly occurs in the boreal spring, the spring warm pool (SWP) is formed in the central SCS. The SWP peaks in May and then decays in June.

[15] Our analyses show that the surface heat flux and ocean dynamics have different roles in the formation and decay of the SWP. Before the onset of the summer southwest monsoon, the sky over the SCS is relatively clear with less cloud cover and rainfall and thus more shortwave radiation can enter into the upper layer ocean. At the same time, the loss of the latent heat flux from the ocean is decreased owing to the weak wind during the monsoon transition period of May. Therefore, the surface heat flux is responsible for forming the SWP in May. During that time, the effect of ocean dynamics is negligible. The onset of the southwest monsoon corresponds to an increase in cloudiness and rainfall and a strong wind speed in the SCS all which decrease the surface heat flux in June. The onset of the southwest monsoon also changes oceanic circulation pattern with a strong southeastward current and an upward entrainment velocity in the central SCS. As a result, the southeastward current advects cold water from the northwest to the southeast, and the upward entrainment velocity on the bottom of mixed layer pumps cold water into the mixed layer. These cooling effects overcome the warming effect of the surface heat flux, resulting in the decay of the SWP in June.

[16] As shown in other studies, the SCS SST anomalies displays a large interannual variation associated with ENSO [e.g., *Klein et al.*, 1999; *Wang et al.*, 2002; *Xie et al.*, 2003; *Wang et al.*, 2006]. Therefore, the SWP may have a large signal on interannual timescale. In addition, what is the role of the SWP in local air-sea interaction? Does the SWP feed back to local atmospheric circulation? These issues and SWP's potential impacts on climate and weather such as rainfall and typhoon over the SCS deserve for further investigations.

References

Chu, P. C., H. Tseng, C. P. Chang, and J. M. Chen (1997), South China Sea warm pool detected in spring from the Navy's Master Oceanographic Observational Data Set (MOODS), *J. Geophys. Res.*, *102*, 15,761–15,768.

Cushman-Roisin, B. (1987), Subduction, paper presented at Hawaiian Winter Workshop, School of Ocean Sci. and Technol., Univ. of Hawai'i at manoa, Honolulu.

He, Y. H., and C. H. Guan (1997), A primary study of the South China Sea warm pool (I), *Res. Dev South China Sea*, *4*, 8–11.

Klein, S. A., B. J. Soden, and N. C. Lau (1999), Remote sea surface variations during ENSO: Evidence for a tropical atmospheric bridge, *J. Clim.*, *12*, 917–932.

Lau, N.-C., and K.-H. Lau (1992), Simulation of the Asian summer monsoon in a 40-year experiment with a general circulation model, *East Asia and Western Pacific Meteorology and Climate*, edited by W. J. Kyle and C. P. Chang, pp. 49–56, World Sci., Hackensack, N. J.

Lau, K. M., K. M. Kim, and S. Yang (2000), Dynamical and boundary forcing characteristics of regional components of the Asian summer monsoon, *J. Clim.*, *13*, 2461–2482.

Levitus, S., and T. Boyer (1994), *World Ocean Atlas 1994*, vol. 4, *Temperature*, NOAA Atlas NESDIS, vol. 4, 129 pp., Natl. Oceanic and Atmos. Admin., Silver Spring, Md.

Liu, Q. Y., D. X. Wang, Y. L. Jia, H. J. Yang, J. L. Sun, and Y. Du (2002), Seasonal variation and formation mechanism of the South China Sea warm water, *Acta Oceanol. Sin.*, *21*, 331–343.

Liu, Q., X. Jiang, S.-P. Xie, and W. T. Liu (2004), A gap in the Indo-Pacific warm pool over the South China Sea in boreal winter: Seasonal development and interannual variability, *J. Geophys. Res.*, *109*, C07012, doi:10.1029/2003JC002179.

Meyers, G., R. J. Bailey, and A. P. Worby (1995), Geostrophic transport of Indonesian Throughflow, *Deep Sea Res., Part I*, *42*, 1163–1174.

Oberhuber, J. M. (1988), An atlas based on the "COADS" data set: The budgets of heat, buoyancy and turbulent kinetic energy at the surface of the global ocean, *Rep. 15*, Max Planck Inst. für Meteorol., Hamburg, Germany.

Qu, T. (2001), The role of ocean dynamics in determining the mean seasonal cycle of the South China Sea surface temperature, *J. Geophys. Res.*, *106*, 6943–6955.

Wang, D. X., Q. Xie, Y. Du, W. Q. Wang, and J. Chen (2002), The 1997–1998 warm event in the South China Sea, *Chin. Sci. Bull.*, *47*, 1221–1227.

Wang, C., W. Q. Wang, D. X. Wang, and Q. Wang (2006), Interannual variability of the South China Sea associated with El Niño., *J. Geophys. Res.*, doi:10.1029/2005JC003333, in press.

Williams, R. G. (1989), The influence of air-sea interaction on the ventilated thermocline, *J. Phys. Oceanogr.*, *19*, 1255–1267.

Xie, S.-P., Q. Xie, D. X. Wang, and W. T. Liu (2003), Summer upwelling in the South China Sea and its role in regional climate variations, *J. Geophys. Res.*, *108*(C8), 3261, doi:10.1029/2003JC001867.

Zhang, Q. R., Y. Du, and D. X. Wang (2001), Shape features of warm water in South China Sea, *J. Trop. Oceanogr.*, *20*, 69–76.

Zhao, Y. P., and Y. L. Chen (2000), The seasonal and inter-annual variability of the South China Sea warm pool and its relation to the South China Sea monsoon onset, *J. Trop. Meteorol.*, *16*, 202–211.

————————————

C. Wang, Physical Oceanography Division, Atlantic Oceanographic and Meteorological Laboratory, NOAA, Miami, FL 33149, USA. (chunzai.wang@noaa.gov)

W. Wang, Key Laboratory of Tropical Marine Environmental Dynamics, South China Sea Institute of Oceanology, Chinese Academy of Sciences, West Xingang Road 164, Guangzhou 510301, China. (weiqiang.wang@noaa.gov)